Available online at www.sciencedirect.com

ScienceDirect

Procedia Engineering 130 (2015) 176 – 192

Procedia Engineering

www.elsevier.com/locate/procedia

14th International Conference on Pressure Vessel Technology

Impact of Bauschinger Effect on the Residual Contact Pressure of Hydraulically Expanded Tube-to-Tubesheet Joints

A.-H. Bouzid[a], A.-H.I. Mourad[b], A. El Domiaty[c,*]

[a]*École de Technologie Supérieure, Montreal, Quebec, Canada*
[b]*Abdel-Hamid I. Mourad, United Arab Emirates University, Al-Ain, UAE*
[c]*Aly El Domiaty, Suez Canal University, Ismailia, Egypt*

Abstract

The level of the contact pressure and the stresses induced during the hydraulically expanded tube–to-tubesheet process are the key factors for the integrity of a leak free expanded joint. The modelling of this type of joint requires an adequate representation of the material behavior in order to accurately evaluate important joint parameters such as the residual contact pressure and induced residual stresses. Maintaining a lower bound safe limit of the initial residual contact pressure over the lifetime of the expanded joint insures its durability. A design tool that addresses a proper material-geometry combination in conjunction with the required expansion pressure is developed.

The proposed model is based on strain hardening material behavior of the tube and the tubesheet. The interaction of these two components is simulated during the whole process of the application of the expansion pressure. Particular emphasis is put on influence of reverse yielding and Bauschinger effect on the residual contact pressure. The results from the analytical model are confronted to those of the numerical FEA model. Two joints of different geometries and materials are considered to demonstrate the importance of considering the real material behavior in both models.

Peer-review under responsibility of the organizing committee of ICPVT-14

Keywords: Tube-to-tubesheet joint, analytical modeling, revese yielding, FE modeling, residual stress;

* Corresponding author. Tel.: +1-514-396-8563; fax: +1-514-396-8530.
E-mail address: hakim.bouzid@etsmtl.ca

Peer-review under responsibility of the organizing committee of ICPVT-14
doi:10.1016/j.proeng.2015.12.187

Nomenclature

A	radius of
B	position of
C	further nomenclature continues down the page inside the text box
ν_t, ν_s	Poisson's ratio of tube and tubesheet
σ_r^t, σ_r^s	Radial stress of tube and tubesheet (MPa)
σ_θ^t, σ_θ^s	Hoop stress of tube and tubesheet (MPa)
σ_z^t, σ_z^s	Axial stress of tube and tubesheet (MPa)
A_t, A_{tu}	Tube loading and unloading plasticity constants (MPa)
A_s, A_{su}	Tubesheet loading and unloading plasticity constants (MPa)
B_t, B_s	Tube loading and unloading strength coefficients (MPa)
B_s, B_{su}	Tubesheet loading and unloading strength coefficients (MPa)
c	Initial clearance (mm)
C, D	Integration constants
E_t, E_{tu}	Tube loading and unloading elastic modulus (MPa)
E_s, E_{su}	Tubesheet loading and unloading elastic modulus (MPa)
n, n_u	Tube loading and unloading strain hardening exponents
m, m_u	Tubesheet loading and unloading strain hardening exponents
p_{at}, p_{as}	Autofrettaged pressure of tube and tubesheet (MPa)
p_c^*	Residual contact pressure (MPa)
p_{yt}, p_{ys}	Pressure to start yield in tube and tubesheet (MPa)
p_c, p_{cm}	Contact pressure and its maximal value (MPa)
p_i, p_e	Expansion pressure and its maximal value (MPa)
r_t, r_s	Tube and Tubesheet elasto-plastic radius (mm)
r_i, r_o	Inner and outer tube radii (mm)
R_i, R_o	Inner and equivalent outer tubesheet radii (mm)
S_{yt}, S_{ytu}	Tube loading and unloading yield stress (MPa)
S_{yt}, S_{ysu}	Tubesheet loading and unloading yield stress (MPa)
U_t, U_s	Radial displacement of tube and tubesheet (mm)
Y_s	Inner to equivalent outer diameter ratio of tubesheet
Y_t	Inner to outer diameter ratio of tube
Y_{tc}, Y_{sc}	Plastic to outer diameter ratio of tube and tubesheet

1. Introduction

Industrial plants such as nuclear, power and chemical plants working under high pressure and high temperature conditions are subjected to leakage, spill ad contamination. This is particularly true for those plants operating with fluids under pressure. The growing concern about the reliability of industrial equipment subjected to mechanical and thermal loading under harsh environment has fostered a lot of research activities in North American and the Gulf

countries. Recent Canadian surveys [1] pointed out to an important source of fugitive emission and contamination in processing plants related to leakage of pressurized equipment such as pressure vessel and piping components, valves and compressors. In addition, the cost of hydrocarbon losses from each equipment were estimated between 200,000 $ to 1 M$ per year.

Tube-to-tubesheet joints used in steam boiler, heat exchanger and steam generators are no exception. Typical failure that may result from improper expansion are leak, stress corrosion cracking, ligament movements, tube extrusion, tube fatigue, ovalling and cracked ligaments[2,3]. Unfortunately, these failures have been reported in many heat exchangers, boilers and steam generators and are attributed to the lack of tube expansion process optimization [4]. The structural integrity and the tightness of tube-to-tube-sheet joints are provided by the residual contact pressure produced mechanically by the method of tube expansion during the manufacture of the tubular equipment. Mechanical rolling, hydraulic expansion and explosive expansion which involve plastic deformation of the materials are the most popular processes used by the industry. The process of expansion consists of expanding the tube so as to close the gap and creates a permanent contact between the tube and tubesheet in order to provide a rigid joint and avoid gross leaks. Usually a small weld around the tube end is added in order to avoid fine leaks. Therefore any fluid transfer between the two circuits is prevented. According to the fundamentals of the expansion process, there are three different zones as shown in Fig. 1; the expanded zone; the transition zone and the unexpanded zone. The first two zones are of concern and have been the subject of little research.

The design and analysis of the expansion process of tube-to-tubesheet joints is not covered by standards such as ASME BPV code [5] and BS5500 [6]. Standards such as TEMA [7] give only basic dimensions of the tubes and the tubesheet holes including clearances. Heat exchanger manufacturers have their own design recipes often based on trial and error are unfortunately not made available in the literature. The expansion process requires optimization in order to insure the desired structural integrity and leak tightness. The ASME BPV code covers the design calculation of tubes and perforated plates separately but not the design involving the actual fabrication process of tube-to-tubesheet expansion. The latter requires a well-documented design methodology coupled to the good engineering practices. The modeling of tube-to-tubesheet joint expansion can be traced back to the paper by Goodier et al. [8] in 1943. Before that the focus of research was on the rigidity of assembly manufactured by mechanical rolling which was the only used process those days. There was no mean to evaluate the interface contact pressure or the residual stresses generated by the roller expansion and trial and error was the best practice. In addition, process defects such dents, local tube deformation and wall thinning were very common. Therefore the weaknesses of this process and the several failures of heat exchangers using these joints have compelled researchers to focus more on the fundamentals of this process and its effects on the joint tightness. However, the research efforts conducted on tube-to-tubesheet expansion together with their use in the steam generators of nuclear power stations have lead Westinghouse in the mid 70's to develop a new process of expansion that uses hydraulic pressure of water or other fluids. This process became quickly the current method of expansion in the nuclear industry. Soon after, the first analytical approach to predict the contact pressure in hydraulically expanded tube-to-tubesheet was developed by Krips et al. [9]. Other researchers have also treated this subject. The different studies cover the three aspects of analysis including the analytical, numerical and experimental works. The developed analytical models and the proposed equations focus on the prediction of the residual contact pressure [10-14]. It is worth noting that all developed models were based on an elastic-perfectly plastic behavior of the tube material. In addition, the combined flexibility of the tube and tubesheet during unloading was not considered. For the more recent models, the validation was conducted using numerical finite element and some adjustments were proposed in some cases [12]. The effect of strain hardening was only evaluated numerically using FEM [15-17] while reverse yielding was not thought to have an effect.

The combined flexibility analysis of the tube and tubesheet during unloading was first introduced Laghzale et al. [18,19] in their analytical model. The authors first treated the case of elastic perfectly plastic of both the tube and tubesheet. Later they incorporated a linear strain hardening in their model. The effect of initial clearance was studied in [16,19]. Recently the creep relaxation behavior of the expanded joint was investigated experimentally [20] in and analytically in [21]. Recently, Huang et al. [22] followed a more realistic approach by introducing a power law in their analytical model but did not account for reverse yielding. The latter is a well-known phenomenon that is the subject of a lot of studies in autofretaged thick cylinders and in the metal forming industry [23-25]. The literature

shows that it has a major influence on the residual stresses. This phenomenon takes also place in thin tubes such as those of expanded joints. Depending on the level of the maximum expansion pressure, the tube can be in reverse yielding after the pressure is release. The compression exerted by the tubesheet has a smaller effect if the tube is in reverse yielding as it becomes less rigid. Therefore ignoring reverse yield would results in higher residual contact pressure and kinetic hardening materials would also produce less contact pressure than their isotropic hardening counterparts. Therefore, due to Bauschinger effect, the contact pressure decreases more rapidly as the expansion pressure is released leading to an overestimation of the residual pressure by existing analytical models. The pull-out tests conducted on expanded joints [26] confirm the above and point to the overestimation of the residual contact pressures by the existing models.

This paper gives the detailed equations of a developed model that estimates the residual contact pressure of a hydraulically expanded tube-to-tubesheet joint based on a kinetic hardening behavior of the tube and tubesheet materials. The model is validated using FEM and comparison with isotropic hardening behavior is conducted on two different material and geometry cases. The importance of the true material behavior is discussed. In addition comparison the effect of strain hardening is investigated by running an elastic perfectly plastic behavior on two cases. In addition to the Tresca and Von Mises yield criteria comparison, the plane strain versus the plane stress is also studied in order to have some idea on the effect of the tubesheet thickness.

2. Analytical Model With Kinematic Strain Hardening

The expanded joint consisting of the tube and tubesheet are often modelled as two concentric cylinders. The tubesheet is therefore replaced by a sleeve with an equivalent external diameter, the expression of which can be given in [26]. The materials for both the tube and tubesheet are considered to follow a power law with a kinematic strain-hardening behavior. In addition only the tube is considered to be in reverse yielding. The loading and unloading are shown in Fig. 1 such that:

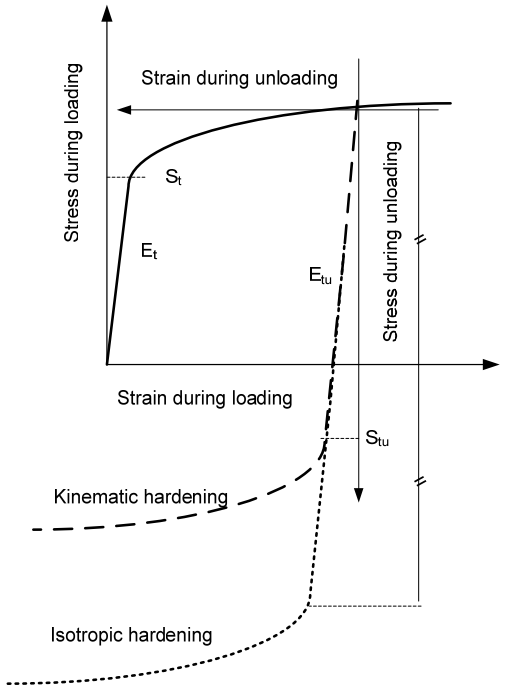

Fig. 1. Material model behavior.

For tube loading and unloading

$$\text{tube}\begin{cases}\sigma = E_t\varepsilon & for\ \sigma \le S_{yt}\\ \sigma = A_t + B_t\varepsilon^{n} & for\ \sigma > S_{yt}\end{cases}\begin{cases}\sigma = E_{tu}\varepsilon & for\ \sigma \le S_{ytu}\\ \sigma = A_{tu} + B_{tu}\varepsilon^{n_u} & for\ \sigma > S_{ytu}\end{cases}\text{ and tubesheet}\begin{cases}\sigma = E_s\varepsilon & for\ \sigma \le S_{ys}\\ \sigma = A_s + B_s\varepsilon^{m} & for\ \sigma > S_{ys}\\ \sigma = E_{su}\varepsilon & for\ all\ \sigma\end{cases} \quad (1)$$

The plastic model is based on Henckey deformation theory and the Von Mises yield criteria is applied. It is supposed that the clearance is relatively big to assume that the tube undergoes full plasticity before it comes into contact with the tubesheet. Depending on the maximum level of the expansion pressure, the geometry and the material properties of the joint, there are three cases that are considered as shown in Fig. 2:

1- Expansion without plastic deformation of the tubesheet and with or without tube partial or full reverse yielding (Fig. 2 steps 1-2-3-a-4-b-7-g-h or …-b-7-g-8-i).

2- Expansion with partial or full plastic deformation of the tubesheet and with or without tube partial or full reverse yielding (Fig. 2 steps 1-2-3-a-4-5-d-7-j-k or …-d-7-j-8-l).

3- Expansion with full plastic deformation of the tubesheet and with or without tube partial or full reverse yielding (Fig. 2 steps 1-2-3-a-4-5-f-7m-n or …-f-7-m-8-o).

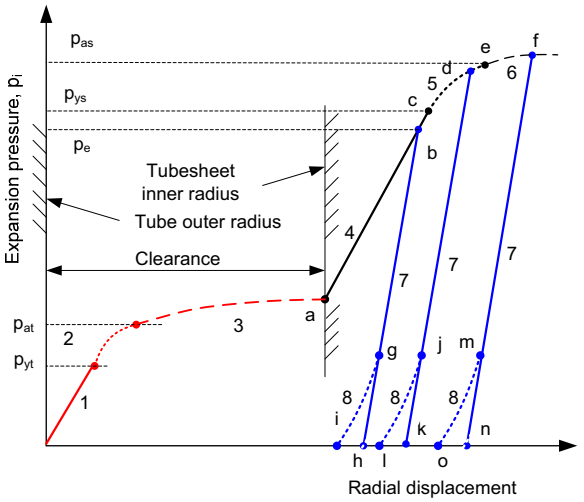

Fig. 2. Expansion pressure sequence.

Under the plane strain condition $\varepsilon_z = 0$, the constitutive equations according to Hencky deformation theory under incompressible volume $\varepsilon_\theta + \varepsilon_r = 0$ in the three directions r, θ and z of a thick cylinder are given by [27]

$$\varepsilon_\theta = \frac{3\varepsilon_e}{4\sigma_e}\left(\sigma_\theta - \sigma_r\right) \quad (2)$$

and

$$\varepsilon_r = \frac{3\varepsilon_e}{4\sigma_e}\left(\sigma_r - \sigma_\theta\right) \quad (3)$$

where σ_e and ε_e are respectively the equivalent stress and strain given by Von Mises criteria

$$\sigma_e = \frac{\sqrt{3}}{2}\left(\sigma_\theta - \sigma_r\right) \tag{4}$$

The compatibility of deformation under plane strain

$$\varepsilon_\theta + \varepsilon_r = 0 \tag{5}$$

And for plane strain the axial stress is given by

$$\sigma_z = \frac{1}{2}\left(\sigma_\theta + \sigma_r\right) \tag{6}$$

2.1. Expansion without tubesheet yielding

To avoid tubesheet plastic deformation, the maximum expansion pressure p_e is to be lower than the pressure p_{ys} at which yield of the tubesheet occurs at the end of the loading phase. Referring to Fig. 2, the loading phase shown under steps 1 and 2 corresponds to the elasto-plastic deformation of the tube. In step 3, the entire tube is fully plastic and at its end the initial gap is closed. In step 4 the tubesheet is elastic deformed. Finally, step 7 represents the unloading phase showing the elastic recovery of the tube and the tubesheet. It is worth noting that the slopes of these lines represent the rigidity of the expanded tube and its capability to resist pressure. Therefore, the slope in step 1 represents the tube rigidity. In step 2, the tube rigidity decreases significantly to and is at its lower value during step 3 in which case the tube resistance to the expansion pressure is reduce considerably. In step 4 the slope represents the combined rigidity of the tube and tubesheet with a predominant contribution from the latter. During the unloading phase, in step 7, the pressure is resisted by both the tube and the tubesheet in which case the slope is higher since full recovery of both the tube and the tubesheet takes place at the same time.

2.1.1. Step 1: Tube elastic deformation

Initially, as the pressure is increased the tube deforms elastically until it reaches yield. According to the Von Mises criteria, the pressure p_{yt} that causes yield is given by:

$$p_{yt} = \frac{S_{yt}}{\sqrt{3}}\frac{Y_t^2 - 1}{Y_t^2} \tag{7}$$

2.1.2. Step 2: Tube elastic-plastic deformation

In step 2, as the pressure is increased above p_{yt}, the tube is partially plastic. Starting with the equilibrium equation of a thick cylinder

$$\frac{d\sigma_r}{dr} + \frac{\sigma_r - \sigma_\theta}{r} = 0 \tag{8}$$

Substituting for $\sigma_r - \sigma_\theta$ by $-2\sigma_e / \sqrt{3}$ from Eq.(4) and noting that σ_e is given by Eq. (1) and integrating gives

$$\int_{r_i}^{r_c} d\sigma_r = \int_{r_i}^{r_c} \frac{2}{\sqrt{3}}\left(A_t + B_t\varepsilon^n\right)\frac{dr}{r} \tag{9}$$

From the geometric equations

$$\varepsilon_\theta = \frac{u}{r} \tag{10}$$

and

$$\varepsilon_r = \frac{du}{dr} \tag{11}$$

Substituting Eq.(10) and (11) into Eq.(5) and integrating gives

$$u = \frac{C}{r} \tag{12}$$

Substitution of Eq.(12) into Eq.(10) and then into Eq.(2) gives

$$\varepsilon_e = \frac{2}{\sqrt{3}} \frac{C}{r^2} \tag{13}$$

Noting that at $r = r_c$, $\varepsilon_e = S_{yt} / E_t$ gives

$$C = \frac{\sqrt{3}}{2} \frac{S_{yt}}{E_t} r_c^2 \tag{14}$$

Substituting Eq.(14) into Eq.(13) and then into Eq.(9) and noting that at $r = r_i$, $\sigma_r = -p_i$ gives the radial stress

$$\sigma_r^t(r) = -p_i + \frac{2A_t}{\sqrt{3}} \ln \frac{r}{r_i} + \frac{B_t}{\sqrt{3}n} \left(\frac{S_{yt}}{E_t} \right)^n \left[\left(\frac{r_c}{r_i} \right)^{2n} - \left(\frac{r_c}{r} \right)^{2n} \right] \tag{15}$$

By putting $\sigma_r^t = 0$ at $r = r_o$ in Eq.(15) gives the pressure that causes a plastic zone of radius r_c is given by:

$$p_{yct} = \frac{2}{\sqrt{3}} A_t \ln Y_t + \frac{B_t}{\sqrt{3}n} \left(\frac{S_{yt}}{E_t} \right)^n \left[\left(\frac{r_c}{r_i} \right)^{2n} - \left(\frac{r_c}{r_o} \right)^{2n} \right] \tag{16}$$

Equation (12) is valid in the elastic zone and can be used to determine the displacement of the tube outside radius as a function of the elastic-plastic interface radius r_c. Substituting for C from Eq.(14) into Eq.(12) and putting $r = r_o$ gives:

$$u_r^t(r_o) = \frac{\sqrt{3}}{2} \frac{S_{yt} r_o}{E_t Y_{tc}^2} \tag{17}$$

The pressure that causes full plasticity in the tube is given by Eq. (16) with $r_c = r_o$ or $Y_{tc} = 1$ such that:

$$p_{at} = \frac{2}{\sqrt{3}} A_t \ln Y_t + \frac{B_t}{\sqrt{3}n}\left(\frac{S_{yt}}{E_t}\right)^n \left(Y_t^{2n} - 1\right) \tag{18}$$

2.1.3. Step 3: Tube plastic deformation and closing of the initial clearance

If p_i is increased beyond p_{at}, Eq.(9) is still valid for the whole tube. Substituting Eq.(13) into Eq.(12) and integrating between r_i and r_o and noting that $\sigma_r^t(r_i) = -p_i$ and $\sigma_r^t(r_o) = 0$ gives the constant C and substituting it into Eq.(12) gives the radial displacement of the tube as

$$u_r^t(r) = \frac{1}{r}\left[\frac{\frac{2n}{B_t}\left(\frac{2A_t}{\sqrt{3}}\ln Y_t - p_i\right)}{\left(\frac{2}{\sqrt{3}}\right)^{n+1}\left(r_o^{-2n} - r_i^{-2n}\right)}\right]^{1/n} \tag{19}$$

And then using Eq.(9) with a back substitution for C and integrating between r_i and r gives the radial stress:

$$\sigma_r^t(r) = \left(p_i - \frac{2A_t}{\sqrt{3}}\ln\frac{r}{r_i}\right)\left[\frac{r^{-2n} - r_i^{-2n}}{r_o^{-2n} - r_i^{-2n}} - 1\right] \tag{20}$$

When the tube comes into contact with the tubesheet the displacement at $r = r_o$ given by Eq.(19) is equal to the clearance c and therefore the pressure required to close the gap is:

$$p_{cg} = \frac{2A_t}{\sqrt{3}}\ln Y_t + \left(\frac{2}{\sqrt{3}}\right)^{n+1} \frac{A_t}{-2n}\left(cr_o\right)^n \left(r_o^{-2n} - r_i^{-2n}\right) \tag{21}$$

2.1.4. Step 4: Elastic deformation of tubesheet

If the pressure is increased after the tube comes into contact with the tubesheet, the former continues to deform plastically while the latter deforms elastically by undergoing the same displacement as the tube. This is shown in step 4 of Fig. 1 from point a to b up to point c. A contact pressure p_c is generated at the interface taking a maximum value of p_{cm} at the maximum expansion value of p_e. The maximum expansion pressure p_e remains lower than the expansion pressure that starts tubesheet yielding, p_{ys}. The case where p_e is higher than p_{ys} will be treated below. During this step, the interface displacement and the stress state can be determined if the contact pressure p_c is known. This is obtained by considering the geometrical compatibility equation of displacement of the tube and tubesheet at their interface where $r_o = R_i$ and is given by:

$$u_r^t(r_o) = c + u_r^s(R_i) \tag{22}$$

The tubesheet radial displacement is given by:

$$u_r^s(r) = \frac{3\,p_c R_o^2}{2E_s\left(Y_s^2 - 1\right)r} \tag{23}$$

Putting $r = R_i$ in Eq.(23) and substituting into Eq.(22) and then into Eq.(12), the constant C is then obtained and therefore after its substitution into Eq.(13) which in turn is substituted in Eq.(9) gives the radial stress as

$$\sigma_r^t(r) = -p_i + \frac{2A_t}{\sqrt{3}}\ln\frac{r}{r_i} - \left(\frac{2}{\sqrt{3}}\right)^{n+1}\frac{B_t r_o^n}{2n}\left(c + \frac{3\,p_c R_o^2}{2R_i E_s\left(Y_s^2 - 1\right)}\right)^n\left(r^{-2n} - r_i^{-2n}\right) \tag{24}$$

The contact pressure p_c is obtained by noting that the radial stress in Eq.(24) is equal to the contact pressure $-p_c$ at the outer radius and solving.

2.2. Expansion with tubesheet plastic deformation

2.2.1. Step 5: Tubesheet elastoplastic deformation

Referring to Fig. 1, the contact pressure p_{cys} required to start tubesheet yielding is given by Eq. (7) replacing the pressure p_{yt}, S_{yt} and Y_t by p_{cys}, S_{ys} and Y_s respectively such that:

$$P_{cys} = \frac{S_{ys}}{\sqrt{3}}\frac{Y_s^2 - 1}{Y_s^2} \tag{25}$$

Substituting Eq.(24) into Eq.(23) gives the expansion pressure required to cause start of yield in the tubeshet

$$p_{ys} = \frac{S_{ys}}{\sqrt{3}}\frac{Y_s^2 - 1}{Y_s^2} + \frac{2A_t}{\sqrt{3}}\ln\frac{r}{r_i} - \left(\frac{2}{\sqrt{3}}\right)^{n+1}\frac{B_t r_o^n}{2n}\left(c + \frac{\sqrt{3}\,S_{ys}R_i}{2E_s}\right)^n\left(r^{-2n} - r_i^{-2n}\right) \tag{26}$$

Equation (17) can also be used to obtain the tubesheet radial displacement:

$$u_r^s(R_i) = \frac{\sqrt{3}}{2}\frac{S_{ys}R_i}{E_s Y_{sc}^2} \tag{27}$$

Equation (27) is inserted into Eq.(22) and then into Eq.(12), the constant C is then obtained. The latter is substituted into Eq.(13) which in turn is substituted in Eq.(9) the integration of which gives the radial stress as

$$\sigma_r^t(r) = -p_i + \frac{2A_t}{\sqrt{3}}\ln\frac{r}{r_i} - \frac{B_t r_o^n}{\sqrt{3}n}\left(\frac{2c}{\sqrt{3}} + \frac{S_{ys}R_c^2}{R_i E_s}\right)^n\left(r^{-2n} - r_i^{-2n}\right) \tag{28}$$

The contact pressure p_c is obtained by noting that the radial stress in Eq.(28) is equal to the contact pressure $-p_c$ at the outer radius. Using the same approach as for the elasto-plastic analysis of the tube, the tubesheet radial stress is given by

$$\sigma_r^s(r) = -p_c + \frac{2A_s}{\sqrt{3}}\ln\frac{r}{R_i} + \frac{B_s}{\sqrt{3}m}\left(\frac{S_{ys}}{E_s}\right)^m\left[\left(\frac{R_c}{R_i}\right)^{2m} - \left(\frac{R_c}{r}\right)^{2m}\right] \tag{29}$$

The radial stress of the tube and tubesheet are equal at the interface radius. Noting that the radial stress is equal to $-p_c$ in Eq.(28) when $r = r_o$ and substituting for $-p_c$ in Eq.(29) and noting that the radial stress of the tubesheet at the radius R_c is equal to zero, the pressure require to cause collapse is obtained

$$p_{as} = \frac{2A_s}{\sqrt{3}} \ln Y_s - \frac{B_s}{\sqrt{3}m} \left(\frac{S_{ys}}{E_s} \right)^m \left[1 - Y_s^{\,2m} \right] + \frac{2A_t}{\sqrt{3}} \ln Y_t - \frac{B_t r_o^n}{\sqrt{3}n} \left(\frac{2c}{\sqrt{3}} + \frac{S_{ys} R_c^2}{E_s R_i} \right)^n \left(r_o^{-2n} - r_i^{-2n} \right) \tag{30}$$

2.2.2. Step 6: Tubesheet plastic deformation

If p_i is increased beyond a certain value the tubesheet will be fully plastic. Substituting Eq.(13) into Eq.(9) and integrating between R_i and R_o and noting that $\sigma_r^t(R_i) = -p_c$ and $\sigma_r^t(R_o) = 0$ gives the constant C and back substitution into Eq.(12) gives the radial displacement of the tubesheet as

$$u_r^s(r) = \frac{1}{r} \left[\frac{p_c - \frac{2A_s}{\sqrt{3}} \ln Y_s}{\left(\frac{2}{\sqrt{3}} \right)^{m+1} \frac{B_s}{-2m} \left(R_o^{-2m} - R_i^{-2m} \right)} \right]^{1/m} \tag{31}$$

Then using Eq.(9) with a back substitution for C and integrating from R_i to r gives the radial stress in the tubesheet:

$$\sigma_r^s(r) = \left(p_c - \frac{2A_s}{\sqrt{3}} \ln \frac{r}{R_i} \right) \left[\frac{r^{-2m} - R_i^{-2m}}{R_o^{-2m} - R_i^{-2m}} - 1 \right] \tag{32}$$

Putting $r = R_i$ in Eq.(31) and substituting into Eq.(22) and then into Eq.(12), the constant C is then obtained and therefore after its substitution into Eq.(13) which in turn is substituted in Eq.(9) gives the radial stress in the tube as

$$\sigma_r^t(r) = -p_i + \frac{2A_t}{\sqrt{3}} \ln \frac{r}{r_i} - \left(\frac{2}{\sqrt{3}} \right)^{n+1} \frac{B_t r_o^n}{2n} \left(r^{-2n} - r_i^{-2n} \right) \left(c + \frac{1}{R_i} \left[\frac{\frac{2m}{B_s} \left(\frac{2A_s}{\sqrt{3}} \ln Y_s - p_c \right)}{\left(\frac{2}{\sqrt{3}} \right)^{m+1} \left(R_o^{-2m} - R_i^{-2m} \right)} \right]^{\frac{1}{m}} \right)^n \tag{33}$$

The contact pressure p_c is obtained by noting that the radial stress in Eq.(33) is equal to the contact pressure $-p_c$ at the outer radius and solving.

2.2.3. Step 7: Unloading without reverse yielding

After reaching its maximum value p_e, the release of pressure involves the simultaneous elastic recovery of the tube and the tubesheet. The contact pressure is obtained by analyzing the change in the radial displacement of the tube and tubesheet at their interface. This change must be the same such that:

$$\Delta u_r^t(r_o) = \Delta u_r^s(R_i) \tag{34}$$

During unloading, the tube relative radial displacement is given by the elastic recovery from the state where it is subjected to the maximal internal and external pressures p_e and p_{cm} and a lower state level where it is subjected to the internal and external pressures p_i and P_c such that:

$$\Delta u_r^t(r) = \frac{3r}{2E_t\left(Y_t^2-1\right)}\left\{\left(p_i-p_e\right)-\left(p_c-p_{cm}\right)\right\} \tag{35}$$

he tubesheet relative radial displacement is given by the elastic recovery from the state where it is subjected to maximal internal contact pressures p_{cm} to the lower state level where it is subjected to the internal pressure p_c such that:

$$\Delta u_r^s(r) = \frac{3Y_s^2 r}{2E_s\left(Y_s^2-1\right)}\left(P_c-P_{cm}\right) \tag{36}$$

Evaluation of Eqs. (35) and (36) at respectively r_o and R_i and substitution into Eq. (34) gives: 、

$$p_c = p_{cm} + \lambda(p_i - p_e) \tag{37}$$

where λ is given by:

$$\lambda = \frac{2}{\frac{E_t R_i\left(Y_t^2-1\right)}{E_s r_o\left(Y_s^2-1\right)}Y_s^2+1} \tag{38}$$

The residual contact pressure p_c^* is given by putting p_i equal to zero in Eq. (37) such that:

$$p_c^* = p_{cm} - \lambda p_e \tag{39}$$

2.2.4. Step 8: Unloading with tube in partial reverse yielding

During unloading, reverse yielding of the tube occurs when the change in stress from the maximum expansion pressure state is greater than the unloading yield stress S_{ytu} which is usually equal to $2S_{yt}$. Equation (15) is applicable for partial reverse yielding by replacing p_i with $p_e - p_i$, S_{yt} by S_{ytu} and E_t by E_{tu} . The case of Kineting hardening with equal loading and unloading properties will be treated in this paper. The radial stress is therefore given by

$$\Delta\sigma_r^t(r) = -p_e + p_i + \frac{2A_{tu}}{\sqrt{3}}\ln\frac{r}{r_i} + \frac{B_{tu}}{\sqrt{3}n_u}\left(\frac{S_{ytu}}{E_{tu}}\right)^{n_u}\left[\left(\frac{r_c}{r_i}\right)^{2n_u} - \left(\frac{r_c}{r}\right)^{2n_u}\right] \tag{40}$$

Equation (17) for the change of radial displacement is also applicable replacing S_{yt} by S_{ytu} and E_t by E_{tu} such that

$$\Delta u_r^t(r) = \frac{\sqrt{3}}{2}\frac{S_{ytu} r_c}{E_{tu} r^2} \tag{41}$$

The change in radial stress at the tube outside radius is equal to the change in contact pressure $p_{cm} - p_c$. Noting that at the start of reverse yielding the change in pressures of a cylinder subjected to internal and external pressure difference is given by Eq.(7). Therefore substituting Eq.(37) into Eq.(7) and replacing the pressure p_{ys} by $(p_e - p_i) - (p_{cm} - p_c)$ and S_{yt} by S_{ytu} gives:

$$p_i = p_e - \frac{\left(Y_t^2 - 1\right)}{\sqrt{3} Y_t^2 \left(1 - \lambda\right)} S_{ytu} \tag{42}$$

2.2.5. Step 9: Unloading with tube in full reverse yielding

Substituting Eq.(13) into Eq.(9) and integrating between r_i and r_o and noting that $\sigma_r^t(r_i) = -P_e$ and $\sigma_r^t(r_o) = -P_c$ gives the constant C and back substitution into Eq.(17) gives the radial displacement of the tubesheet as:

$$\Delta u_r^t\left(r\right) = \frac{1}{r}\left[\frac{p_c - p_{cm} - p_i + p_e - \frac{2A_{tu}}{\sqrt{3}}\ln Y_t}{\left(\frac{2}{\sqrt{3}}\right)^{n_u+1}\frac{B_{tu}}{-2n_u}\left(r_o^{-2n_u} - r_i^{-2n_u}\right)}\right]^{1/n_u} \tag{43}$$

The radial stress changes is given by

$$\Delta\sigma_r^t\left(r\right) = -p_e + p_i + \frac{2A_{tu}}{\sqrt{3}}\ln\frac{r}{r_i} - \left(r^{-2n_u} - r_i^{-2n_u}\right)\left(\frac{p_c - p_{cm} - p_i + p_e - \frac{2A_{tu}}{\sqrt{3}}\ln Y_t}{\left(r_o^{-2n_u} - r_i^{-2n_u}\right)}\right) \tag{44}$$

The contact pressure p_c is obtained by noting that the radial stress in Eq.(45) is equal to the contact pressure $-p_c$ at the outer radius and solving.

3. Numerical Finite Element Modeling

The validation of the analytical model was conducted by direct comparison of the stresses, radial displacements and the contact pressures with their FE model counterpart using ANSYS software [29]. Plane strain elements PLANE183 with eight nodes and two degrees of freedom per node (2 displacements) were used to model the tube and the tubesheet as shown in Fig. 4. Elements CONTA72 and TARG169 were also deployed to model the contact surfaces of the tube and the tubesheet. Although a small angle portion could have been used to model the expanded joint, a 90 degree portion was model for simplicity. Conditions of plane of symmetry are applied to the edge nodes of the cut planes. The geometrical and mechanical characteristics of the two studied joints are obtained from the literature [19,22] and are shown in Table 1. The effect of plain stress versus plane strain was investigated by selecting the proper element option when required. Also the effect of the material behavior was look at by setting the option MKIN for multilinear kinematic hardening, MISO multilinear isotropic hardening, BKIN (Bilinear kinematic) or BISO (Bilinear isotropic) for the elastic perfect plastic case.

A mesh refinement convergence criterion based on less than 1% on the residual contact pressure was implemented. The FE plane model presented in Fig 4 was preferred to an axisymmetrical model because it is simple

to generate and faster to resolve. Previous studies [12-14, 5] conducted on similar expanded joints showed that there is no significant difference between plane stress and axisymmetric models when studying contact pressure and deformation. Similarly, friction between the tube and tubesheet is not affected by the type of model used. In practice distilled or purified water is used as the pressure fluid in order to avoid surface flaking or spalling due to lubrication.

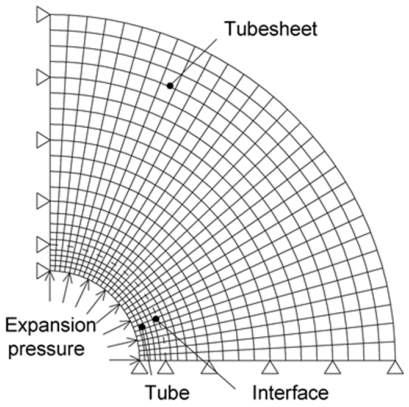

Fig. 3. Plane strain FE model.

Table 1. Geometry and material properties.

	Case 1 [18]		***Case 2 [12]***	
	Tube	*Tubesheet*	*Tube*	***Tubesheet***
r_o, R_o***(mm-in)***	12.5-0.492	21.5-0.846	9.525-0.375	17.5-0.689
r_i, R_i ***(mm-in)***	10.5-0.413	12.7-0.5	8.24-0.324	9.627-0.379
E_t, E_s	190.4 27608	206.8	294	199.6
(GPa-ksi)		29986	42630	28942
S_{yt}, S_{ys}	205	347	248	422
(MPa-ksi)	29.73	50.32	35.96	61.19
ν_t, ν_s	0.3	0.3	0.289	0.289
A_t, A_s	67.6	314.3	280,	0,
(MP-ksi)	9.8	45.57	40.6	0
B_t, B_s	790.05	998.1	626	871
(MPa-ksi)	114.56	144.73	90.77	126.3
n, m	0.2694	0.632	0.46	0.117
P_e ***(MPa-ksi)***	290- 42.05		370- 53.65	
C (mm-in)	0.2- 0.008		0.126- 0.005	

4. Results and Discussion

The developed analytical model went through a rigorous stress analysis comparison with its numerical FEM counterpart before the current investigation on the material behavior was launched. Stresses, deformations and contact pressure as a function of the hydraulic pressure variation during the expansion process were compared. As a sample of the comparison, Figs. 4 and 5 show the variation of the interface contact pressure and the radial displacement of the tube outside diameter with the application of the expansion pressure. The graphs show the

results of the two expanded joints cases 1 and 2 detailed in Table 1 and subjected to a maximum expansion pressure of 260 and 340 MPa respectively. These two parameters are depicted during the two loading and unloading phases of the expansion process. The variation of the contact pressure is 10% when the expansion pressure is at its maximum value and around 17% when the pressure is released for case 2. Case 1 shows better results since these differences are only 5.1 and 1.2%. Although the difference in the displacement between the two methods is shown to be significant when the tube reaches full plasticity without contacting the tubesheet during the loading phase, the final values are only 1.3 and 2.2%. This indicates that Henckey deformation theory gives acceptable results as compared to the more accurate incremental theory used by the FEM software. It is worth noting that there are the different segments the slope of which represents the rigidity the expanded joint which changes depending on the step phase of the expansion process. A straight segment indicates that both joint elements are elastic and curved segment indicates that either or both elements are deformed plastically. In particular, the last curved segment during unloading indicates that reverse yielding is present in case 1.

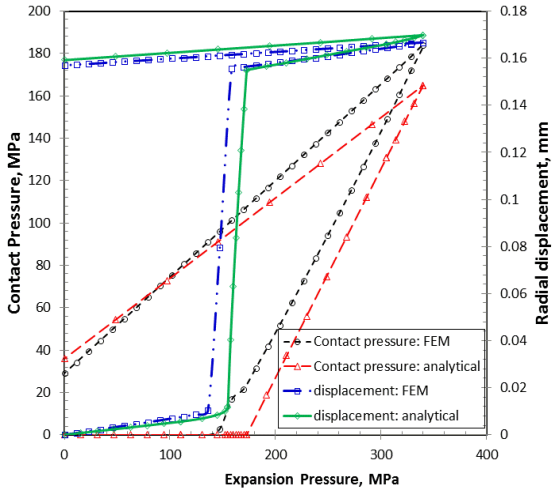

Fig. 4. Variation of the contact pressure during expansion: Case 1 with pe=260 MPa (37.7 ksi).

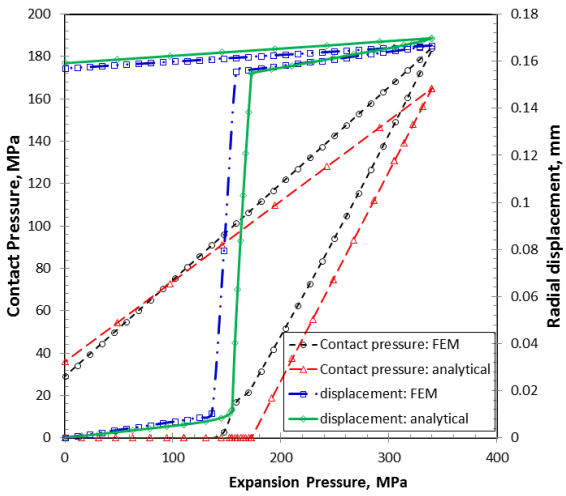

Fig. 5. Variation of contact pressure during expansion: Case 2 with pe=340 MPa (49.3 ksi).

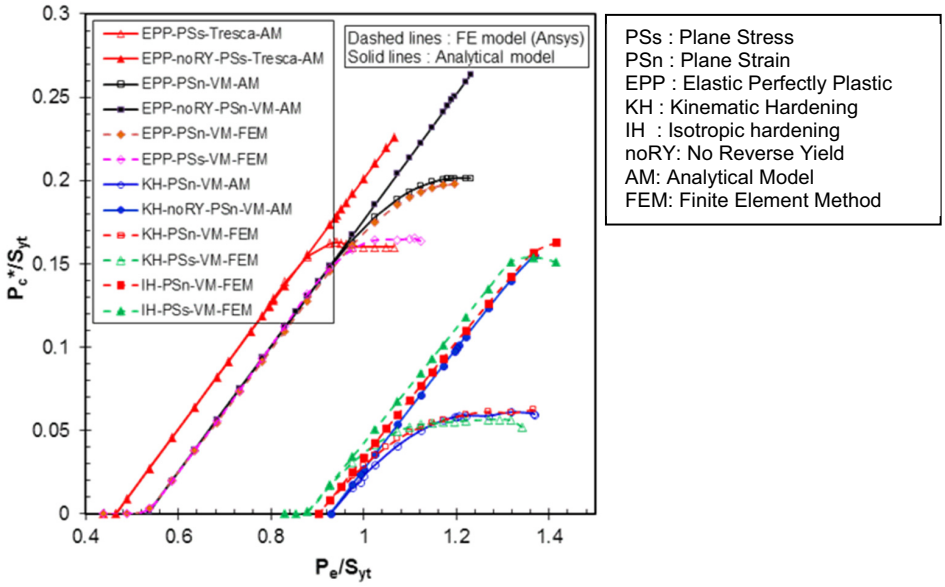

Fig. 6. Residual contact pressure variation as a function of expansion pressure; Case 1.

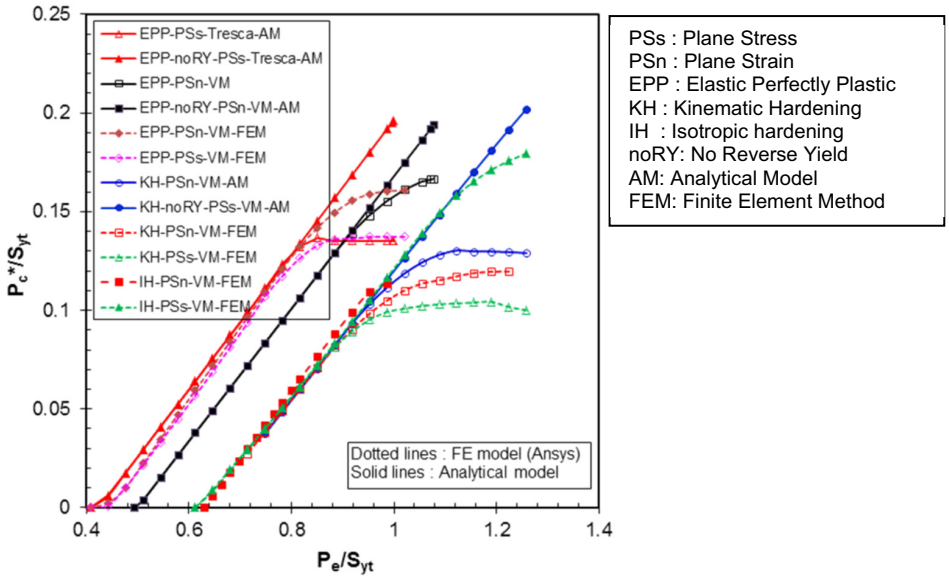

Fig. 7. Residual contact pressure variation as a function of expansion pressure; Case 2.

Figures 6 and 7 give the normalized residual contact pressure as a function of the normalized maximum expansion pressure with reference to the tube yield stress. The normalized residual contact pressures were evaluated for plane strain and stress, the hardening yield surface model, elastic perfectly plastic material for both Tresca and Von Mises. The plane strain analytical model was run with and without reverse yielding. Fundamentally there is no

difference between kinetic hardening and isotropic hardening when no reverse yielding occurs. However, when the latter takes place the difference is significant and ignoring it would lead to a none-conservative approach. In fact, the difference in the prediction of the residual contact pressure can be more than twice.

The elastic perfectly plastic case predicts the lowest expansion pressures followed by the kinematic hardening case and finally the isotropic hardening case. The difference between plane strain and plane stress is not significant as in the case with the residual contact pressure. These curves can give an idea on the limiting pressure to avoid reverse yielding and achieve higher residual contact pressures. This study shows that reverse yielding affects the residual contact pressure in tube-to-tubesheet joint expansion. The developed model predicts the maximum expansion pressure at which it can be avoided.

5. Conclusion

The importance of a proper modelling of hydraulically expanded tube-to-tubesheet joint is demonstrated in this paper. The Bauschinger effect is a factor the needs to be considered when producing expanded joints since it affects their structural integrity. The developed analytical model was validated against FEA at the different stages of the expansion process and was found to give a good estimate of residual contact pressures and stresses in hydraulically expanded joints. It can also be used as analytical tool to help achieve optimum expanded joint material and geometry configurations.

This paper puts emphasis on the importance of the effect of hardening yield surface, strain hardening and yield criteria. Isotropic hardening and Tresca predict twice more residual contact pressure for the same expansion pressure. The FEM study showed no significant difference between plane strain and plane stress in the evaluation of the residual contact pressure.

Acknowledgements

The authors acknowledge the help received by Mehdi Kazeminia PhD student at Ecole de Technologie Superieure during the development of the FE model using the numerical software. Ansys.

References

[1] A. Chambers,Well Test Flare Plume Monitoring:-Results of DIAL Measurements in Alberta, Carbon and Energy Management, Alberta Research Council Inc., PTAC Air Issues Forum, November 19, 2003.

[2] D. Rochester, A. McIlree, J.P. Molkenthin, T.P. Magee, J.F. Hall, G.C. Fink, Unique Primary Side Initiated Degradation in the Vicinity of the Upper Roll Transition in once through Steam Generators from Oconee Unit 1, Proc. of the 9th International Symposium on Environmental Degradation of Materials in Nuclear Power Systems - Water Reactors -, (1999) 133–140.

[3] L. Cizelj, B. Mavko, Crack Propagation in Residual Stress Dominated Steam Generator Tube Expansion Transition Zones, Proc. of the Meeting on Nuclear Energy: Central Europe: Present and Perspectives, (1993) 228–235.

[4] Z.F. Sang, Y.Z. Zhu, G.E.O. Widera, Reliability Factors and Tightness of Tube-to-Tubesheet Joints, ASME J. Pressure Vessel Technol. 118 (1996) 137–41.

[5] ASME, ASME Section VIII Div. 1, Boiler and Pressure Vessel Code, ASME, NY, 2013.

[6] CEN, EN13445, Unfired Pressure Vessels, CEN, 2007

[7] Standards of the Tubular Exchanger Manufacturers Association, , 8th ed., the Tubular Manufacturers Association, Tarrytown, New York, 1999.

[8] J.N. Goodier, G.J. Schoessow, The Holding Power and Hydraulic Tightness of Expanded Tube Joints: Analysis of the Stress and Deformation, Trans. ASME, 65-5 (1943) 489–496.

[9] H. Krips, M. Podhorsky, Hydraulisches Aufweiten Em Dash Ein Neues Verfahren Zur Befestigung Von Rohren," VGB Kraftwerkstechnik, 56-7(1976) 456–464.

[10] S. Yokell, Welded-and-Expanded Tube-to-Tubesheet Joints, ASME J. Pressure Vessel Technol., 114 (1992) 157–165.

[11] W.R. Kohlpaintner, Calculation of Hydraulically Expanded Tube-to-Tubesheet Joints," ASME Journal of Pressure Vessel Technology, 117 (1995) 24–30.

[12] Allam, M., Chaaban, A. and Bazergui, 1998, "Estimation of residual stresses in hydraulically expanded tube-to-tubesheet joints," Journal of Pressure Vessel Technology, 120, 1998, p 129–137.

[13] M.H. Jawad, E.J. Clarkin, R.E. Schuessler, Evaluation of Tube-to-Tubesheet Junctions,'' ASME Journal Pressure Vessel Technology, 109 (1987) 19–26.
[14] D.K. Williams, Comparison of Residual Stresses in the Mechanical Roll Expansion of HX Tubes Into TEMA Grooves," ASME Journal of Pressure Vessel Technology, 129 (2007) 324–241.
[15] D. Updike, A. Kalnins, S. Caldwell, Elastic Plastic Analysis of Tube Expansion in Tubesheets, ASME J. Pressure Vessel Technol., 114 (1992) 149–156.
[16] N. Merah, A. Al-Zayer, A. Shuaib, A. Arif, A., Finite Element Evaluation of Clearance Effect on Tube-to-Tubesheet Joint Strength, Internl. Journal of Pressure Vessels and Piping, 80-12 (2003) 879–885.
[17] M. Allam, A. Bazergui, A. Chaaban, The effect of tube strain hardening level on the residual contact pressure and residual stresses of hydraulically expanded tube-to-tubesheet joint, Proc. of the ASME Pressure Vessel and Piping Conference, 375 (1998) 447–455.
[18] N. Laghzale, A. Bouzid, Analytical Modelling of Hydraulically Expanded Tube-to-Tubesheet Joints, ASME Journal of Pressure Vessel Technology, 131-1 (2009) 011208–9
[19] N. Laghzale, A. Bouzid, Theoretical Analysis of Hydraulically Expanded Tube-To-Tubesheet Joints with Linear Strain Hardening Material Behavior," ASME Journal of Pressure Vessel Technology, 131-6 (2009) 061202–8
[20] C.B. Bahn, S. Majumdar, K.E Kasza, W.J. Shack, Leak Behavior of Steam Generator Tube-to-Tubesheet Joints under Creep Condition: Experimental Study, International Journal of Pressure Vessels and Piping, 101 (2003) 55–63.
[21] N. Laghzale, Bouzid A., Effect of Creep on the Residual Stresses in Tube-to-Tubesheet Joints, ASME Journal of Pressure Vessel Technology, 132-6 (2010) 061210–6
[22] X. Huang, T. Xie, Modeling Hydraulically Expanded Tube-to-Tubesheet Joint Based on General Stress-Strain Curves of Tube and Tubesheet Materials, Journal of Pressure Vessel Technology, 133-3 (2011) 031205–9
[23] P.C.T. Chen, Bauschinger and hardening effects on residual stresses in autofrettaged thick-walled cylinders," ASME Journal Pressure Vessel Technology, 108 (1986) 108–112
[24] A.P. Parker, J.H. Underwood, Influence of the Bauschinger effect on residual stresses and fatigue lifetimes in autofrettaged thick-walled cylinders," ASTM Special Technical Publication, 1332 (1999) 565–583.
[25] P. Livieri, P. Lazzarin, Autofrettaged Cylindrical Vessels and Bauschinger Effect: An Analytical Frame for Evaluating Residual Stress Distributions, ASME J. Pressure Vessel Technology, 124 (2002) 38–46.
[26] M. Allam A. Bazergui, Axial Strength of Tube-to-Tubesheet Joints: Finite Element And Experimental Evaluations," Journal of Pressure Vessel Technology, Transactions of the ASME, 124 (2002) 22–31.
[27] A. Chaaban, H. Ma, A. Bazergui, Tube-Tubesheet Joint: A Proposed Equation for the Equivalent Sleeve Diameter Used in the Single Tube Model, ASME J. Pressure Vessel Technology, 114 (1992) 19–22
[28] X. Gao, An Exact Elasto-Plastic Solution for an Open-Ended Thick-Walled Cylinder of a Strain-Hardening Material," International Journal of Pressure Vessels & Piping, 52 (1992) 129–44.
[29] ANSYS, ANSYS Structural Analysis Guide, v. 9, 2004.